Sun Weijie (Orcid ID: 0000-0001-5260-658X)
Slavin James A. (Orcid ID: 0000-0002-9206-724X)
Tian Anmin (Orcid ID: 0000-0002-4351-551X)
Poh Gangkai (Orcid ID: 0000-0002-5775-2006)
Akhavan-Tafti Mojtaba (Orcid ID: 0000-0003-3721-2114)
Lu San (Orcid ID: 0000-0003-2248-5072)
Yao Shutao (Orcid ID: 0000-0002-6059-2963)
Le Guan (Orcid ID: 0000-0002-9504-5214)
Nakamura Rumi (Orcid ID: 0000-0002-2620-9211)
Giles Barbara L. (Orcid ID: 0000-0001-8054-825X)
Burch James L (Orcid ID: 0000-0003-0452-8403)

MMS study of the structure of ion-scale flux ropes in the Earth's cross-tail current sheet

W. J. Sun [1], J. A. Slavin [1], A. M. Tian [2], S. C. Bai [2], G. K. Poh [3,4], M. Akhavan-Tafti [1], S. Lu [5], S. T. Yao [2], G. Le [3], R. Nakamura [6], B. L. Giles [3], J. L. Burch [7].

[1] Department of Climate and Space Sciences and Engineering, University of Michigan, Ann Arbor, MI 48109, USA

[2] Shandong Provincial Key Laboratory of Optical Astronomy and Solar-Terrestrial Environment, School of Space Science and Physics, Shandong University, Weihai, 264209, China

[3] NASA Goddard Space Flight Center, Greenbelt, Maryland 20771, USA

[4] Center for Research and Exploration in Space Sciences & Technology II, University of Maryland Baltimore County, Baltimore, Maryland 21250, USA

[5] Department of Earth, Planetary, and Space Sciences, University of California, Los Angeles, California, USA

[6] Space Research Institute, Austrian Academy of Sciences, Graz, Austria

[7] Southwest Research Institute, San Antonio, Texas, USA

E-mail: wjsun@umich.edu

This is the author manuscript accepted for publication and has undergone full peer review but has not been through the copyediting, typesetting, pagination and proofreading process, which may lead to differences between this version and the Version of Record. Please cite this article as doi: 10.1029/2019GL083301

Key Points,

1. Ion-scale flux ropes are observed to have either flattened or circular cross-sections using MDD and GS reconstruction.
2. Analysis of 25 flux ropes show circular cross-section flux ropes have stronger core field and smaller thermal pressures than flattened flux ropes.
3. The two types of flux ropes may be the results of reconnection, temporal evolution, or interactions with external environment.

Abstract.
This study analyzes 25 ion-scale flux ropes in the Magnetospheric Multiscale (MMS) observations to determine their structures. The high temporal and spatial resolution MMS measurements enable the application of multi-spacecraft techniques to ion-scale flux ropes. Flux ropes are identified as quasi-one-dimensional (quasi-1D) when they retain the features of reconnecting current sheets, i.e. the magnetic field gradient is predominantly northward or southward, and quasi-2D when they exhibit circular cross-sections, i.e., the magnetic field gradients in the plane transverse to the flux rope axis are comparable. The analysis shows that the quasi-2D events have larger core fields and smaller pressure variations than the quasi-1D events. These two types of flux ropes could be the result of different processes, including magnetic reconnection with different dawn-dusk magnetic field components, temporal transformation of flattened structure to circular, or interactions with external environments.

Keywords. Ion-scale FRs, Magnetic Structure, Plasma Depletion, Evolution

Plain Language Summary.
Magnetic flux ropes are fundamental magnetic structures in space plasma physics, and are commonly seen in the universe, such as, astrophysical jets, coronal mass ejections (CMEs), and planetary magnetospheres. Flux ropes are important in mass and energy transport across plasma and magnetic boundaries, and they are found in a wide range of spatial sizes, from several tens of kilometers, i.e., ion-scale flux ropes, to tens of million kilometers, i.e., CMEs, in the solar system. The ion-scale flux ropes can be formed during magnetic reconnection and are hypothesized to energize electrons and influence the reconnection rate. Previous examinations of the structure of ion-scale flux ropes were greatly limited by measurement resolution. The unprecedented Magnetospheric Multiscale (MMS) mission high temporal and spatial resolution measurements provide a unique opportunity to investigate flux rope structures. By employing multi-spacecraft techniques, this study has provided new insights into the magnetic field variations and dimensionality of ion-scale flux ropes in the Earth's magnetotail. The results are

consistent with the evolution of ion-scale flux ropes from initially flattened current sheet-like flux ropes near the time of formation into lower energy state with circular cross-section predicted by theory and termed as the “Taylor” state.

1. Introduction

Magnetic flux ropes, or plasmoids, were first proposed to be formed in the Earth's magnetotail between the distant tail magnetic reconnection line (X-line) and the near-Earth X-line with scale of few to several tens of Earth's radii (R_E) [*Schindler*, 1974; *Hones*, 1977]. Later studies using the measurements of ISEE-3 and Geotail revealed the presence of smaller flux ropes with diameters of the order of 10^5 km [*Hones et al.*, 1984; *Slavin et al.*, 1989, 2003a; *Ieda et al.*, 1998; *Zong et al.*, 1997, 1998]. The small-scale flux ropes were proposed to be formed due to the tearing mode instability in reconnecting current layers. The smallest flux ropes were found to be on scales of only a few ion inertial lengths [*Drake et al.*, 2006a]. Hereafter, we refer to them as "ion-scale flux ropes". Some simulations indicated that component reconnection controlled formation of ion-scale flux rope [*Drake et al.*, 2006b], while other simulations suggested that ion-scale flux ropes could also be formed during anti-parallel reconnection [*Daughton et al.*, 2006; *Markidis et al.*, 2013]. In previous observations, Cluster observed ion-scale flux ropes in the Earth's magnetotail, and they were sometimes accompanied by energetic electrons (> 30 keV) [*Chen et al.*, 2007; *Eastwood et al.*, 2007; *Wang et al.*, 2010]. However, due to the limitation of spatial and time resolutions of measurements, detailed examination of structure of ion-scale flux ropes remains lacking.

MMS mission [*Burch et al.*, 2016] was launched on 13 March 2015 UTC and consists of four identical spacecraft providing high temporal resolution measurements of 3D plasma distributions [*Pollock et al.*, 2016] and high spatial resolution measurements (~ 20 km inter-spacecraft separation). MMS studies near the dayside magnetopause have revealed several interesting features on the ion-scale flux transfer events-type flux ropes, including intense current filaments inside the structures [*Eastwood et al.*, 2016; *Liu et al.*, 2018], evolution in scale [*Dong et al.*, 2017; *Akhavan-Tafti et al.*, 2018] and force balance [*Zhao et al.*, 2016]. There are also several studies of the ion-scale flux ropes in the MMS plasma sheet measurements. For example, *Stawarz et al.* [2018] reported an electron-scale vortex inside a flux rope, and *Teh et al.* [2018] showed that flux rope axes were tilted towards the reconnecting field.

The MMS high-resolution multi-point measurements offer a unique opportunity to apply multi-spacecraft techniques to ion-scale flux ropes. In this work, we first present two case studies followed by a statistical investigation of an ensemble of 25 ion-scale flux ropes. The primary objective is to determine the magnetic field dimensionality and the structure of ion-scale flux ropes in the Earth's cross-tail current sheet. Our results show that ion-scale flux ropes could have either flattened or circular cross-sections. Flux ropes with circular cross-sections have stronger core fields, fewer particles and are embedded in environments with larger dawn-dusk field compared to the flattened flux ropes.

2. Case Studies

2.1. Instrumentations and Techniques

MMS measurements during mission phase 2b from 1 May 2017 to 31 August 2017 with an apogee of ~ 25 R_E were used to identify ion-scale flux ropes in Earth's magnetotail. This survey utilizes the measurements from the fluxgate magnetometers (FGM) [*Russell et al.*, 2016] and the fast plasma investigation (FPI) [*Pollock et al.*, 2016]. In burst mode, the FGM provides magnetic field measurements at 128 vectors/s and the FPI provides 3D electron and ion measurements with energy range of ~ 0.01 to 30 keV/q at time resolutions of 30 ms and 150 ms, respectively. Unless stated otherwise, spacecraft position and vector quantities are given in the Geocentric solar magnetospheric (GSM) coordinates.

The Minimum Directional Derivative or Difference, (MDD) method [*Shi et al.*, 2005] is employed to determine the magnetic field variations and to characterize the dimensionality of the flux ropes. The Spatio-temporal Difference (STD) method [*Shi et al.*, 2006] is used in combination of the MDD to obtain a reference frame for each flux rope. The MDD and STD techniques have been applied to multi-point observations of Cluster [e.g., *Shi et al.*, 2009a, 2009b; *Sun et al.*, 2010; *Li et al.*, 2016] and MMS [e.g., *Hasegawa et al.*, 2017; *Yao et al.*, 2017; *Denton et al.*, 2018]. Local magnetic curvature

of magnetic field lines is obtained by magnetic field rotation analysis [*Shen et al.*, 2007]. Reconstruction of flux ropes using plasma and magnetic field data have been carried out by Grad-Shafaranov (GS) reconstruction [*Sonnerup and Guo*, 1996; *Hau and Sonnerup*, 1999; *Hu and Sonnerup*, 2002; *Tian et al.*, 2018].

2.2. MMS Observations of two Cases

Figure 1 shows MMS observations of two ion-scale flux ropes in the cross-tail current sheet. The left column (Figures 1a to 1j) shows an earthward traveling flux rope at ~ 08:34:11 UT on 6 July 2017 when MMS was located at ~ [-22.1, 3.1, 3.0] R_E. The right column (Figures 1k to 1t) shows a tailward traveling flux rope at ~ 16:45:55 UT on 20 July 2017 when MMS was located at ~ [-23.6, 6.6, 3.6] R_E. In both cases, MMS was located in the central plasma sheet based upon high fluxes of ions and electrons with energies higher than 1 keV (Figures 1c, 1d, 1m, and 1n) and ion beta larger than 1 (Figures 1j and 1t). Ambient $|B_x|$ was small (< 5 nT, Figures 1a and 1k) indicating that MMS crossed near the central axes of the flux ropes.

The July 6 case was embedded in an earthward plasma flow with speed up to ~ 800 km/s (Figure 1e). It had a clear bipolar B_z from negative to positive and a B_t enhancement in the center (Figures 1a and 1b). The maximum B_y inside the flux rope was ~ 10.2 nT, which is ~ 0.47 when normalized to the lobe field (B_{Lobe}). The B_{Lobe} was obtained through pressure balance between the plasma sheet and the lobe [e.g., *Xing et al.*, 2010; *Sun et al.*, 2017]. Dawn-dusk field component surrounding the flux rope (B_{y0}) was ~ 5 nT, i.e., B_{y0} / B_{Lobe} ~ 0.23. The dawn-dusk field is defined as the reconnection's out-of-plane magnetic field component, which could contain both guide field and Hall field [e.g., *Daughton et al.*, 2011; *Nakamura et al.*, 2016]. Plasma density showed a small amplitude increase (~ 6%, Figure 1g) and thermal pressure increased from ~ 0.19 to 0.23 nPa inside the structure. The error flag from FPI burst mode indicates that there is no significant (>25%) hot plasma population (>30 keV) for this event. The July 20 case was embedded in a tailward plasma flow (~ 180 km/s, Figure 1o), and showed a clear polarity change of B_z from positive to negative and a B_t increase in the center. The maximum B_y inside this flux

rope was ~ 17.1 nT (B_{core}/ B_{Lobe} ~ 0.53), and the ambient dawn-dusk field (B_{y0}) was ~ 12 nT (B_{y0}/ B_{Lobe} ~ 0.37) which are both larger than the July 6 case. Contracting to the July 6 case, plasma density was strongly depleted (~ -36%, Figure 1q) inside the July 20 case.

2.3. Dimensionality and Magnetic Field Variations from MDD

During the encounters with the two ion-scale flux ropes in Figure 1, the MMS inter-spacecraft separations were ~ 20 km, much smaller than the scale of the flux ropes (~ 1000 km), and the quality factor (TQF) for the tetrahedral formation were ~ 0.863 and ~ 0.966 [*Robert et al.*, 1998; *Fuselier et al.*, 2016], respectively, indicating that the tetrahedron was regular and was suitable for application of multi-spacecraft techniques. The magnetic field measurements from the four spacecraft are nearly identical for the flux ropes (Figures 2a to 2d and 2i to 2l). In Figures 2e and 2m, the local curvature of magnetic field lines ($\vec{b} \cdot \nabla \vec{b}$, where $\vec{b}$ is magnetic field unit vector) reversed in both the *X* and *Y* components inside the flux ropes. Specifically, the magnetic curvature reversed from -*X* to +*X* for the July 6 case and from +*X* to -*X* for the July 20 case. These confirm helical field configurations of the flux ropes. Meanwhile, the local magnetic curvatures show minima in the center regions, i.e., near the B_z reversal points, marking no or low degree of twist in the core magnetic field. These features of magnetic curvature are consistent with the magnetic field variation of flux ropes showed in previous studies [*Slavin et al.*, 2003a; *Shen et al.*, 2007; *Zhang et al.*, 2013], and the inward magnetic tension balances the outward pressure (both magnetic field and particle) gradient force.

The MDD method was applied to analyze the dimensionality and the magnetic field variations of the two flux ropes (Figures 2f to 2h and 2n to 2p). This method starts from the definition of dimensionality and aims to find the minima of $(\partial B_x/\partial n)^2 + \left(\partial B_y/\partial n\right)^2 + (\partial B_z/\partial n)^2$, where $\vec{n}$ is a certain direction [*Shi et al.*, 2005]. Following procedures of the Minimum Variance Analysis (MVA) method [*Sonnerup and Scheible*, 1998], it comes to solve a symmetrical matrix $\left(\nabla\vec{B}\right)\left(\nabla\vec{B}\right)^T$, where $\left(\nabla\vec{B}\right)^T$ is the transpose of $\nabla\vec{B}$. With four simultaneous spacecraft measurements, MDD is able to give the

eigenvalues and the eigenvectors of this symmetrical matrix with the same cadence as magnetic field measurements. Magnitudes of the three eigenvalues $\sqrt{\lambda_{max}}$, $\sqrt{\lambda_{mid}}$, and $\sqrt{\lambda_{min}}$ (|nT/km|), represent intensities of magnetic field variations along $\vec{n}_{max}$, $\vec{n}_{mid}$, and $\vec{n}_{min}$, respectively. Relative magnitude of the eigenvalues could reveal the dimensionality of magnetic structures.

The eigenvalues for the July 6 case (Figure 2f) show that $\sqrt{\lambda_{max}}$ are at least 5 times $\sqrt{\lambda_{mid}}$, indicating that the magnetic field variation along the maximum eigenvector ($\vec{n}_{max}$, Figure 2g) is much larger than the other two directions. Therefore, this flux rope is quasi-one-dimensional (quasi-1D). The $\vec{n}_{max}$ is mostly along the $\hat{z}_{GSM}$ close to the normal of cross-tail current sheet, indicating that the structure retains the feature of reconnecting current sheet. The eigenvalues for the July 20 case (Figure 2n) show that $\sqrt{\lambda_{mid}}$ and $\sqrt{\lambda_{max}}$ are comparable ($\sqrt{\lambda_{mid}}$ / $\sqrt{\lambda_{max}}$ ~ 0.65), and around an order of magnitude larger than the $\sqrt{\lambda_{min}}$, indicating that this flux rope is quasi-2D. The $\vec{n}_{max}$ (Figure 2o) for this event is mostly along the $\hat{z}_{GSM}$, implying that this flux rope also retains the feature of reconnecting current sheet. The axial directions, i.e., $\vec{n}_{min}$ in Figures 2h and 2p, of the two flux ropes are close to the $\hat{y}_{GSM}$, with the July 20 case being slightly tilted toward the $\hat{x}_{GSM}$.

2.4. GS Reconstruction

The GS reconstruction technique [*Sonnerup and Guo*, 1996; *Hau and Sonnerup*, 1999] was applied to validate the magnetic structure of ion-scale flux ropes determined by the MDD. The application of GS reconstruction on flux ropes requires following assumptions: i) structure can be deemed as time-independent in a proper frame; ii) magnetic field gradient along the axial direction is smaller than those in the other two directions, i.e., in reconstructed plane; iii) structure is quasi-magnetohydrostatic during spacecraft crossing. Under the above assumptions, GS equation can be introduced, $\partial^2 A/\partial T^2 = -\mu_0\, dP_t/dA$, where A is the partial magnetic field vector potential in the plane (T) transverse to the axis, $P_t = P_{th} + B_Y^2/2\mu_0$ is transvers pressure, P_{th} is thermal

pressure. In this equation, both axial magnetic field, B_Y, and P_t are functions of A alone. MDD [*Shi et al.*, 2005] and STD [*Shi et al.*, 2006] are used to build local coordinate system and to find reference frame of the flux ropes. The basic assumption of STD is that magnetic field variations in the spacecraft measurement is due to the motion of magnetic structure, $\left(\partial\vec{B}/\partial t\right)_{sc} = \vec{V}_{str} \cdot \left(\nabla\vec{B}\right)$. The reconstruction plane for the July 6 case is $\vec{X}$=[-0.96, -0.29, 0.030], $\vec{Z}$=[-0.0042, 0.12,0.99] and for the July 20 case event is $\vec{X}$=[0.87, -0.47, 0.11], $\vec{Z}$=[-0.10, 0.038, 0.99]. The reference frame velocity of the July 6 case and the July 20 case are [811, -24, -61] km/s and [-116, 58, -3] km/s, respectively.

The magnetic field vector potential (A_0) in Figures 3a and 3d is obtained by integrating B_Z along the spacecraft trajectory in the plane transverse to the axial direction. The P_t and B_Y are obtained directly from the MMS measurements. Figures 3a and 3d show the polynomial fit of the P_t and A_0 for the two flux ropes. Upon determining P_t(A) and taking the magnetic field measurements along the spacecraft trajectory as initial values, A in the transverse plane is determined by extrapolation. The distributions of P_{th} and B_Y can then be obtained from the functional relations of P_{th}(A) and B_Y(A). The reconstructed B_Y and P_{th} for the two flux ropes are shown in Figure 3. The measured magnetic field components (white arrows) closely align with the reconstructed field lines (black contour) in both events. B_Y increases in the center of both flux ropes (Figures 3b and 3e), while P_{th} increases for the July 6 case (Figure 3c) and decreases for the July 20 case (Figure 3f).

For reference, white circles with radius of 200 km are draw in the center of the flux ropes (Figures 3b and 3e). It is clear that magnetic field lines in the center of the July 6 case largely deviates from the white circle with the magnetic field variation being steeper in the vertical direction ($\vec{Z}$) than in the horizontal direction ($\vec{X}$). The magnetic structure elongates in $\vec{X}$ making its transverse magnetic field component (Figure 3b) close to a one dimensional current sheet, which confirms the quasi-1D structure determined by the MDD. Magnetic field lines are close to the white circle for the July 20 case (Figure 3e),

indicating that the magnetic field variations are similar in the $\vec{Z}$ and $\vec{X}$ directions. The circular cross-section of this flux rope in the plane transverse to the axis confirms the quasi-2D structure determined by the MDD.

3. Statistical Results

Two ion-scale flux ropes in the Earth's cross-tail current sheet were investigated by multi-spacecraft analyses and GS reconstruction and were found in quasi-1D and quasi-2D, respectively. Both flux ropes showed normal direction along $\hat{z}_{GSM}$ and axes mostly along $\hat{y}_{GSM}$. The quasi-2D flux rope contained larger core field (B_{core} / B_{Lobe} ~ 0.53) and was surrounded by a larger dawn-dusk field (B_{y0} / B_{Lobe} ~ 0.37) compared to the quasi-1D flux rope (B_{core} / B_{Lobe} ~ 0.47, B_{y0} / B_{Lobe} ~ 0.23). The particle density increased in the quasi-1D flux rope (~ 6%) while decreased in the quasi-2D flux rope (~ -36%). This section statistically investigates the above features of ion-scale flux ropes.

We have surveyed the FGM and FPI burst mode measurements to identify ion-scale flux ropes in the plasma sheet using the following criteria:

i) the events must be surrounded by $|B_x| < 5$ nT,

ii) the B_z bipolar signature coincides closely with the enhancements of B_y and B_t,

iii) the scale of the flux ropes should be < 10 di,

iv) local magnetic curvature is bipolar along $\vec{X}$ inside the flux ropes.

In this manner, we have identified a total of 25 ion-scale flux ropes. Seven flux ropes are tailward traveling (TFRs), and the other 18 are Earthward traveling (EFRs). Scales of most of the flux ropes are larger than 1di and only 2 are smaller than 1 di.

Figures 4a and 4c show distributions of $\hat{n}_{max}$ and $\hat{n}_{min}$ with flux rope locations in the planes of X_{GSM}-Z_{GSM} and X_{GSM}-Y_{GSM}, respectively. The $\hat{n}_{max}$ is rotated to be positive along $\hat{z}_{GSM}$, and $\hat{n}_{min}$ positive along $\hat{y}_{GSM}$. The $\hat{n}_{max}$ were close to $\hat{z}_{GSM}$ in most of the events (Figure 4a), which is evident in the histogram of separation angles between $\hat{n}_{max}$ and $\hat{z}_{GSM}$ (Figure 4b). The few events with $\hat{n}_{max}$ largely deviating from the $\hat{z}_{GSM}$ are mostly EFRs, which could be deformed due to the strong dipole magnetic field [*Slavin et*

al., 2003a; see also, *Lu et al.*, 2015; *Vogiatzis et al.*, 2015]. The $\hat{n}_{min}$, i.e., the axial directions, were close to $\hat{y}_{GSM}$ with small deviations (Figures 4c and 4d), which is similar to the large scale (~R_E) flux ropes [*Slavin et al.*, 2003a, 2003b].

The flux ropes were divided into two categories according to average eigenvalue ratios between $\sqrt{\lambda_{mid}}$ and $\sqrt{\lambda_{max}}$, in which ratios of quasi-1D flux ropes are smaller than 0.4 and quasi-2D flux ropes larger than 0.4 (see supplementary material). We obtained 13 quasi-1D flux ropes and 12 quasi-2D flux ropes. For the 13 quasi-1D flux ropes, 11 are EFRs and only 2 are TFRs. For the 12 quasi-2D flux ropes, 7 are EFRs and 5 are TFRs. It seems that TFRs are more likely to be quasi-2D, while EFRs tend to be quasi-1D. Figures 4e to 4g show the scatter plots for ambient dawn-dusk field (B_{y0}/B_{Lobe}), core field (B_{core}/B_{Lobe}), and thermal pressure changes ($\Delta P_{th}/P_{th}$). The thermal pressure changes were mostly contributed by the variations of particle densities. These plots show that the quasi-2D flux ropes (red dots) have larger core field (~ 0.59) than the quasi-1D flux ropes (blue dots, ~ 0.40), the decrease of thermal pressure inside quasi-2D flux ropes (~ -0.22) were more prominent than that of quasi-1D flux ropes (~ -0.12). We conclude that the quasi-2D flux ropes have stronger thermal pressure gradient than the quasi-1D flux ropes. Moreover, the quasi-2D flux ropes were observed in environments with relatively larger dawn-dusk field (~ 0.33) than the quasi-1D flux ropes (~ 0.15).

4. Conclusions and Discussions

This study used MMS plasma and magnetic field measurements and multi-spacecraft techniques to investigate magnetic structures of 25 ion-scale flux ropes in the Earth's cross-tail current sheet. The local magnetic curvature of the flux ropes clearly reached a minimum in the center and then reversed direction, demonstrating the helical magnetic field lines inside the flux ropes. MDD analysis has determined that these flux ropes have either flattened (quasi-1D, 13 cases) or circular (quasi-2D, 12 cases) cross-sections. GS reconstruction was applied to one example from each category, which confirmed the MDD characterization of the two types of flux rope structures. For most of the flux ropes, the largest magnetic field variation was along $\hat{z}_{GSM}$, implying that they still retain the

features of reconnecting current sheet, in which they most likely formed. The axial directions of the flux ropes mainly point in $\hat{y}_{GSM}$, but with small tilts toward $\hat{x}_{GSM}$.

The quasi-2D ion-scale flux ropes with circular cross-sections are closer to the lower energy state cylindrical force-free flux ropes [e.g., *Taylor*, 1986] than the quasi-1D flux ropes with flattened cross-sections. The statistical results show that the quasi-2D flux ropes contain stronger core field and lower plasma pressure than the quasi-1D flux ropes (Figure 4e). These results suggest that the newly formed ion-scale flux ropes have already demonstrated distinct properties in the magnetic structures and plasma features. These two groups of ion-scale flux ropes may have been formed by several processes. The quasi-2D flux ropes were observed in regions with a larger dawn-dusk field (~ 0.33) than the quasi-1D flux ropes (~ 0.15) (Figures 4f and 4g), which suggests that magnetic reconnections under these different magnetic field conditions might have given rise to the two different groups of ion-scale flux ropes. Previous studies suggested that flux ropes containing less particles and stronger core fields reached a later stage of the evolution [e.g., *Ma et al.*, 1994; *Chen et al.*, 2017; *Akhavan-Tafti et al.*, 2018], which may suggest that the quasi-2D flux ropes in this study are in the later stage of evolution than the quasi-1D flux ropes. Electric field may be induced during this temporal transformation, which can energize particles and impact the tail dynamic. Furthermore, the different structures might reveal the time history of magnetic reconnections which generate the flux ropes. Lastly, the structures of ion-scale flux ropes can also be influenced by the external environments. EFRs may experience different dipole magnetic field intensity than TFRs, which can influence the structure of flux ropes and cause TFRs to have a characteristic quasi-2D structure. In our statistical results, 11 of the 18 EFRs are quasi-1D while only 2 of the 7 TFRs are quasi-1D.

In summary, the structures of ion-scale flux ropes were analyzed using the MMS measurements. The flux ropes could be either in flattened (quasi-1D) or circular cross-sections (quasi-2D). Flux ropes with circular cross-sections tend to contain stronger core fields and fewer particles than flattened flux ropes. The formation of the two types of ion-

scale flux ropes could be the result of generation by magnetic reconnection with different dawn-dusk magnetic fields, transformation of flattened structures to circular, or interactions with external environments.

Acknowledgements

This work was supported by NASA MMS GI grant 80NSSC18K1363. This research was supported by the NASA MMS in association with NASA contract NNG04EB99C. Institut de Recherche en Astrophysique et Planétologie (IRAP) contributions to MMS FPI were supported by Centre National d'Études Spatiales (CNES) and Centre National de la Recherche Scientifique (CNRS). The data presented in this paper are the L2 data of MMS and can be accessed from MMS Science Data Center (https://lasp.colorado.edu/mms/sdc/public/). We thank the MMS team for data access and support. Wei-Jie Sun thanks Shan Wang (University of Maryland), Yi-Hsin Liu (Dartmouth College), Quanqi Shi (Shandong University), Takuma Nakamura (Austrian Academy of Sciences) and Zuyin Pu (Peking University) for the helpful discussions.

References List

1. Akhavan -Tafti, M., et al. (2018), *Journal of Geophysical Research: Space Physics*, *123*(2), 1224-1241, doi:10.1002/2017JA024681.
2. Burch, J. L., T. E. Moore, R. B. Torbert, and B. L. Giles (2016), Magnetospheric Multiscale Overview and Science Objectives, *Space Science Reviews*, *199*(1), 5-21, doi:10.1007/s11214-015-0164-9.
3. Chen, L. J., et al. (2007), Observation of energetic electrons within magnetic islands, *Nature Physics*, *4*, 19, doi:10.1038/nphys777.
4. Chen, Y., et al. (2017), Global Three-Dimensional Simulation of Earth's Dayside Reconnection Using a Two-Way Coupled Magnetohydrodynamics With Embedded Particle-in-Cell Model: Initial Results, *Journal of Geophysical Research: Space Physics*, 122(10), 10,318-310,335, doi:doi:10.1002/2017JA024186.
5. Daughton, W., V. Roytershteyn, H. Karimabadi, L. Yin, B. J. Albright, B. Bergen, and K. J. Bowers (2011), Role of electron physics in the development of turbulent magnetic reconnection in collisionless plasmas, *Nature Physics*, *7*, 539, doi:10.1038/nphys1965.
6. Daughton, W., J. Scudder, and H. Karimabadi (2006), Fully kinetic simulations of undriven magnetic reconnection with open boundary conditions, *Physics of Plasmas*, *13*(7), 072101, doi:10.1063/1.2218817.
7. Denton, R. E., et al. (2018), Determining L -M - N Current Sheet Coo From Magnetospheric Multiscale Data, *Journal of Geophysical Research: Space Physics*, *123*(3), 2274-2295, doi:10.1002/2017JA024619.
8. Dong, X.-C., et al. (2017), Structure and evolution of flux transfer events near dayside magnetic reconnection dissipation region: MMS observations, *Geophysical Research Letters*, *44*(12), 5951-5959, doi:doi:10.1002/2017GL073411.
9. Drake, J. F., M. Swisdak, H. Che, and M. A. Shay (2006a), Electron acceleration from contracting magnetic islands during reconnection, *Nature*, *443*, 553, doi:10.1038/nature05116
10. Drake, J. F., M. Swisdak, K. M. Schoeffler, B. N. Rogers, and S. Kobayashi (2006b), Formation of secondary islands during magnetic reconnection, *Geophysical Research Letters*, *33*(13), doi:10.1029/2006GL025957.
11. Eastwood, J. P., et al. (2016), Ion-scale secondary flux ropes generated by magnetopause reconnection as resolved by MMS, *Geophysical Research Letters*, *43*(10), 4716-4724, doi:10.1002/2016GL068747.
12. Eastwood, J. P., T. D. Phan, F. S. Mozer, M. A. Shay, M. Fujimoto, A. Retinò, M. Hesse, A. Balogh, E. A. Lucek, and I. Dandouras (2007), Multi-point observations of the Hall electromagnetic field and secondary island formation during magnetic reconnection, *Journal of Geophysical Research: Space Physics*, *112*(A6), doi:10.1029/2006JA012158.
13. Fuselier, S. A., W. S. Lewis, C. Schiff, R. Ergun, J. L. Burch, S. M. Petrinec, and K. J. Trattner (2016), Magnetospheric Multiscale Science Mission Profile and Operations, *Space Science Reviews*, *199*(1), 77-103, doi:10.1007/s11214-014-0087-x.

14. Hasegawa, H., et al. (2017), Reconstruction of the electron diffusion region observed by the Magnetospheric Multiscale spacecraft: First results, *Geophysical Research Letters*, *44*(10), 4566-4574, doi:doi:10.1002/2017GL073163.
15. Hau, L. N., and B. U. Ö. Sonnerup (1999), Two-dimensional coherent structures in the magnetopause: Recovery of static equilibria from single-spacecraft data, *Journal of Geophysical Research: Space Physics*, *104*(A4), 6899-6917, doi:10.1029/1999JA900002.
16. Hu, Q., and B. U. Ö. Sonnerup (2002), Reconstruction of magnetic clouds in the solar wind: Orientations and configurations, *Journal of Geophysical Research*, 107(A7), doi:10.1029/2001JA000293.
17. Hones, E. W. (1977), Substorm processes in the magnetotail: Comments on 'On hot tenuous plasmas, fireballs, and boundary layers in the Earth's magnetotail' by L. A. Frank, K. L. Ackerson, and R. P. Lepping, *Journal of Geophysical Research*, *82*(35), 5633-5640, doi:doi:10.1029/JA082i035p05633.
18. Hones, E. W., Birn, J., Baker, D. N., Bame, S. J., Feldman, W. C., McComas, D. J., ... & Tsurutani, B. T. (1984). Detailed examination of a plasmoid in the distant magnetotail with ISEE 3. Geophysical Research Letters, 11(10), 1046-1049.
19. Hu, Q., and B. U. O. Sonnerup (2003), Reconstruction of two-dimensional structures in the magnetopause: Method improvements, *Journal of Geophysical Research*, 108(A1), 1011, doi:10.1029/2002JA009323.
20. Ieda, A., S. Machida, T. Mukai, Y. Saito, T. Yamamoto, A. Nishida, T. Terasawa, and S. Kokubun (1998), Statistical analysis of the plasmoid evolution with Geotail observations, *Journal of Geophysical Research: Space Physics*, *103*(A3), 4453-4465, doi:10.1029/97JA03240.
21. Li, Z.-Y., W.-J. Sun, X.-G. Wang, Q.-Q. Shi, C.-J. Xiao, Z.-Y. Pu, X.-F. Ji, S.-T. Yao, and S.-Y. Fu (2016), An EMHD soliton model for small-scale magnetic holes in magnetospheric plasmas, *Journal of Geophysical Research: Space Physics*, *121*(5), 4180-4190, doi:doi:10.1002/2016JA022424.
22. Liu, Y., et al. (2018), Ion-scale structures in flux ropes observed by MMS at the magnetopause (in Chinese). *Chin. J. Space Sci.*, 38(2), 147-168, doi:10.11728/cjss2018.02.147
23. Lu, S., Q. Lu, Y. Lin, X. Wang, Y. Ge, R. Wang, M. Zhou, H. Fu, C. Huang, M. Wu, et al. (2015), Dipolarization fronts as earthward propagating flux ropes: A three [illegible] simulation, *Journal of Geophysical Research: Space Physics*, 120, 6286–6300, doi:10.1002/2015JA021213.
24. Ma, Z. W., Otto, A., & Lee, L. C. (1994). Core magnetic field enhancement in single X line, multiple X line and patchy reconnection. *Journal of Geophysical Research*, 99(A4), 6125–6136. https://doi.org/10.1029/93JA03480
25. Markidis, S., P. Henri, G. Lapenta, A. Divin, M. Goldman, D. Newman, and E. Laure (2013), Kinetic simulations of plasmoid chain dynamics, *Physics of Plasmas*, *20*(8), 082105, doi:10.1063/1.4817286.
26. Nakamura, T. K. M., Nakamura, R., Narita, Y., Baumjohann, W., and Daughton, W. (2016). Multi-scale structures of turbulent magnetic reconnection. *Physics of Plasmas*, 23(5), 052116.

27. Pollock, C., et al. (2016), Fast Plasma Investigation for Magnetospheric Multiscale, *Space Science Reviews*, *199*(1), 331-406, doi:10.1007/s11214-016-0245-4.
28. Robert, P., M. W. Dunlop, A. Roux, and G. Chanteur (1998), Accuracy of current density determination, in *Analysis methods for multi-spacecraft data*, edited by G. Paschmann and P. W. Daly, pp. 395-418, ESA Publication, Noordwijk, Netherlands.
29. Russell, C. T., et al. (2016), The Magnetospheric Multiscale Magnetometers, *Space Science Reviews*, *199*(1), 189-256, doi:10.1007/s11214-014-0057-3.
30. Schindler, K. (1974), A theory of the substorm mechanism, *Journal of Geophysical Research*, *79*(19), 2803-2810, doi:doi:10.1029/JA079i019p02803.
31. Shen, C., X. Li, M. Dunlop, Q. Q. Shi, Z. X. Liu, E. Lucek, and Z. Q. Chen (2007), Magnetic field rotation analysis and the applications, *Journal of Geophysical Research: Space Physics*, *112*(A6), doi:10.1029/2005JA011584.
32. Shi, Q. Q., et al. (2009a), Spatial structures of magnetic depression in the Earth's high-altitude cusp: Cluster multipoint observations, *Journal of Geophysical Research: Space Physics*, *114*(A10), doi:10.1029/2009JA014283.
33. Shi, Q. Q., C. Shen, M. W. Dunlop, Z. Y. Pu, Q. G. Zong, Z. X. Liu, E. Lucek, and A. Balogh (2006), Motion of observed structures calculated from multi-point magnetic field measurements: Application to Cluster, *Geophysical Research Letters*, *33*(8), doi:10.1029/2005GL025073.
34. Shi, Q. Q., C. Shen, Z. Y. Pu, M. W. Dunlop, Q. G. Zong, H. Zhang, C. J. Xiao, Z. X. Liu, and A. Balogh (2005), Dimensional analysis of observed structures using multipoint magnetic field measurements: Application to Cluster, *Geophysical Research Letters*, *32*(12), doi:10.1029/2005GL022454.
35. Shi, Q. Q., et al. (2009b), Cluster observations of the entry layer equatorward of the cusp under northward interplanetary magnetic field, *Journal of Geophysical Research: Space Physics*, *114*(A12), doi:10.1029/2009JA014475.
36. Slavin, J. A., et al. (1989), CDAW -8 observations of plasr assessment, *Journal of Geophysical Research*, 94, 15,153
37. Slavin, J. A., R. P. Lepping, J. Gjerloev, D. H. Fairfield, M. Hesse, C. J. Owen, M. B. Moldwin, T. Nagai, A. Ieda, and T. Mukai (2003a), Geotail observations of magnetic flux ropes in the plasma sheet, *Journal of Geophysical Research: Space Physics*, *108*(A1), SMP 10-11-SMP 10-18, doi:10.1029/2002JA009557.
38. Slavin, J. A., et al. (2003b), Cluster electric current density measurements within a magnetic flux rope in the plasma sheet, Geophys. Res. Lett., 30, 1362, doi:10.1029/2002GL016411
39. Sonnerup, B. U. Ö., and M. Guo (1996), Magnetopause transects, *Geophysical Research Letters*, *23*(25), 3679-3682, doi:10.1029/96GL03573.
40. Sonnerup, B. U. Ö., and M. Scheible (1998), Minimum and maximum variance analysis, in *Analysis methods for multi-spacecraft data*, edited by G. Paschmann and P. W. Daly, pp. 185-220, ESA Publication, Noordwijk, Netherlands.

41. Stawarz, J. E., et al. (2018), Intense Electric Fields and Electron-Scale Substructure Within Magnetotail Flux Ropes as Revealed by the Magnetospheric Multiscale Mission, *Geophysical Research Letters*, *45*(17), 8783-8792, doi:10.1029/2018GL079095.
42. Sun, W., et al. (2010), Statistical research on the motion properties of the magnetotail current sheet: Cluster observations, *Science China Technological Sciences*, *53*(6), 1732-1738, doi:10.1007/s11431-010-3153-y.
43. Sun, W. J., et al. (2017). Plasma sheet pressure variations in the near-Earth magnetotail during substorm growth phase: THEMIS observations. *Journal of Geophysical Research: Space Physics*, 122, 12,212–12,228. https://doi.org/10.1002/2017JA024603
44. Taylor, J. B. (1986), Relaxation and magnetic reconnection in plasmas, *Reviews of Modern Physics*, *58*(3), 741-763, doi:10.1103/RevModPhys.58.741.
45. Teh, W. L., T. Nakamura, R. Nakamura, and T. Umeda (2018), Oblique ion-scale magnetotail flux ropes generated by secondary tearing modes, *Journal of Geophysical Research: Space Physics*, *0*(ja), doi:10.1029/2018JA025775.
46. Tian, A., Q. Shi, A. W. Degeling, S. Bai, S. Yao, and S. Zhang (2018), Analytical model test of methods to find the geometry and velocity of magnetic structures, *Science China Technological Sciences*, doi:10.1007/s11431-018-9350-1.
47. Vogiatzis, I. I., Isavnin, A., Zong, Q.-G., Sarris, E. T., Lu, S. W., and Tian, A. M. (2015), Dipolarization fronts in the near-Earth space and substorm dynamics, *Ann. Geophys.*, 33, 63-74.
48. Wang, R., Q. Lu, A. Du, and S. Wang (2010), In Situ Observations of a Secondary Magnetic Island in an Ion Diffusion Region and Associated Energetic Electrons, *Physical Review Letters*, *104*(17), 175003, doi:10.1103/PhysRevLett.104.175003.
49. Xing, X., Lyons, L. R., Nishimura, Y., Angelopoulos, V., Donovan, E., Spanswick, E., … Auster, U. (2011). Near-earth plasma sheet azimuthal pressure gradient and associated auroral development soon before substorm onset. Journal of Geophysical Research, 116, A07204.
50. Yao, S. T., et al. (2017), Observations of kinetic-size magnetic holes in the magnetosheath, *Journal of Geophysical Research: Space Physics*, *122*(2), 1990-2000, doi:doi:10.1002/2016JA023858.
51. Zhang, Y. C., et al. (2013), Two different types of plasmoids in the plasma sheet: Cluster multisatellite analysis application, *Journal of Geophysical Research: Space Physics*, *118*(9), 5437-5444, doi:10.1002/jgra.50542.
52. Zhao, C., et al. (2016), Force balance at the magnetopause determined with MMS: Application to flux transfer events, *Geophys. Res. Lett.*, 43, 11,941–11,947, doi:10.1002/2016GL071568.
53. Zong, Q. -G., et al. (1997), Geotail obser
plasmoid structures in the course of an isolated substorm event, J. Geophys. Res., 102(A6), 11409–11428, doi:10.1029/97JA00076.
54. Zong, Q. -G., et al. (1998), Energetic
intense substorms: Three case studies, J. Geophys. Res., 103(A9), 20339–20363, doi:10.1029/97JA01146.

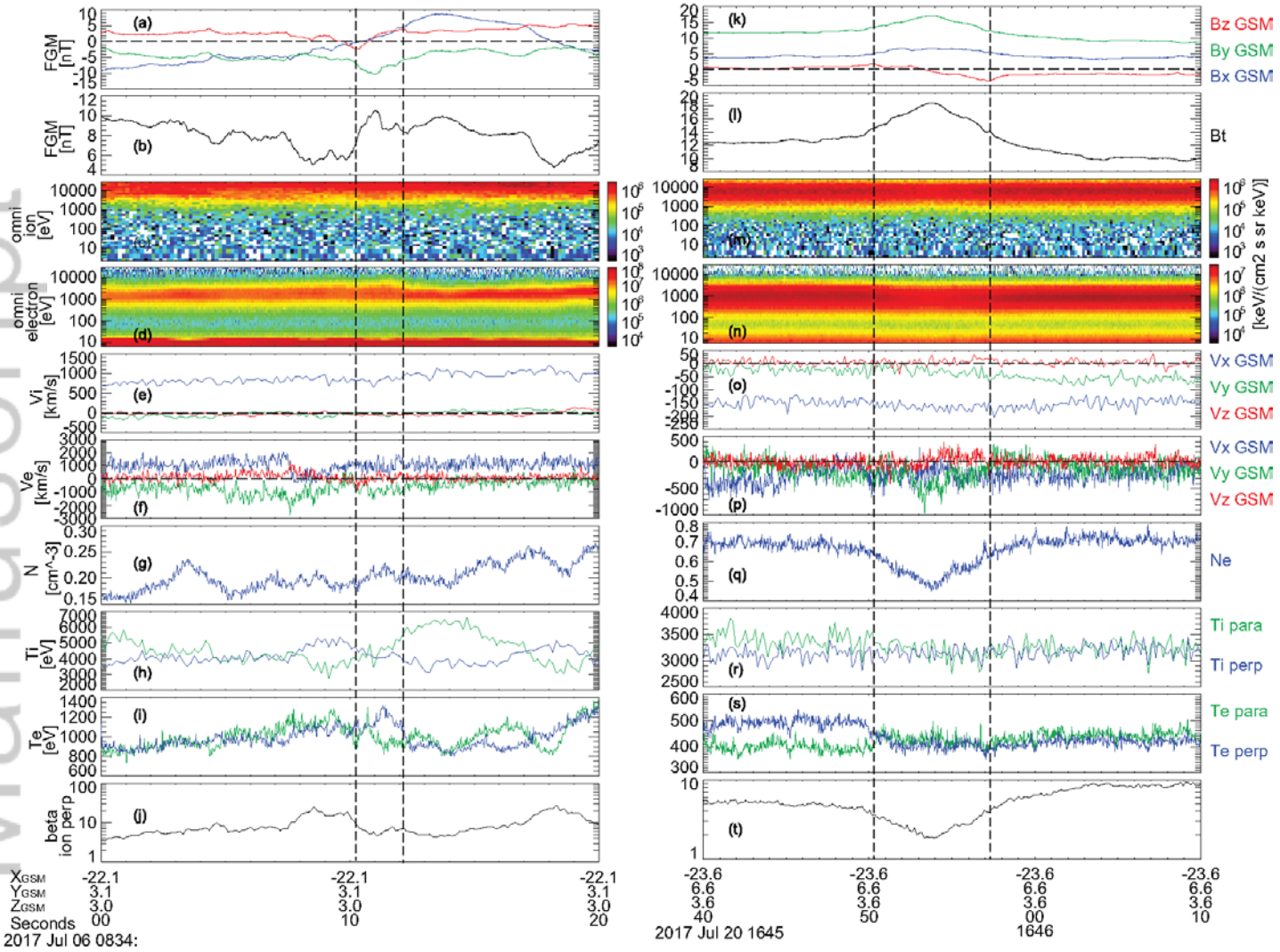

Figure 1. MMS observations of two ion-scale flux ropes in the plasma sheet. July 6 flux rope is shown in left column and July 20 flux rope is shown in right column. (a) and (k), magnetic field components, B_x (blue), B_y (green), and B_z (red). (b) and (l), B_t. (c) and (m), energy spectra of ions. (d) and (n), energy spectra of electrons. (e) and (o), ion bulk velocity, V_x (blue), V_y (green), and V_z (red). (f) and (p), electron bulk velocity. (g) and (q), plasma density (from electron density, N_e). (h) and (r), ion temperature, T_{ipara} (green), T_{iperp} (blue). (i) and (s), electron temperature. (g) and (t), plasma beta calculated from $N_e k_B T_{iperp} / \frac{B_t^2}{2\mu_0}$, where k_B the Boltzmann constant. The vertical dashed lines in each case confined the flux rope central regions.

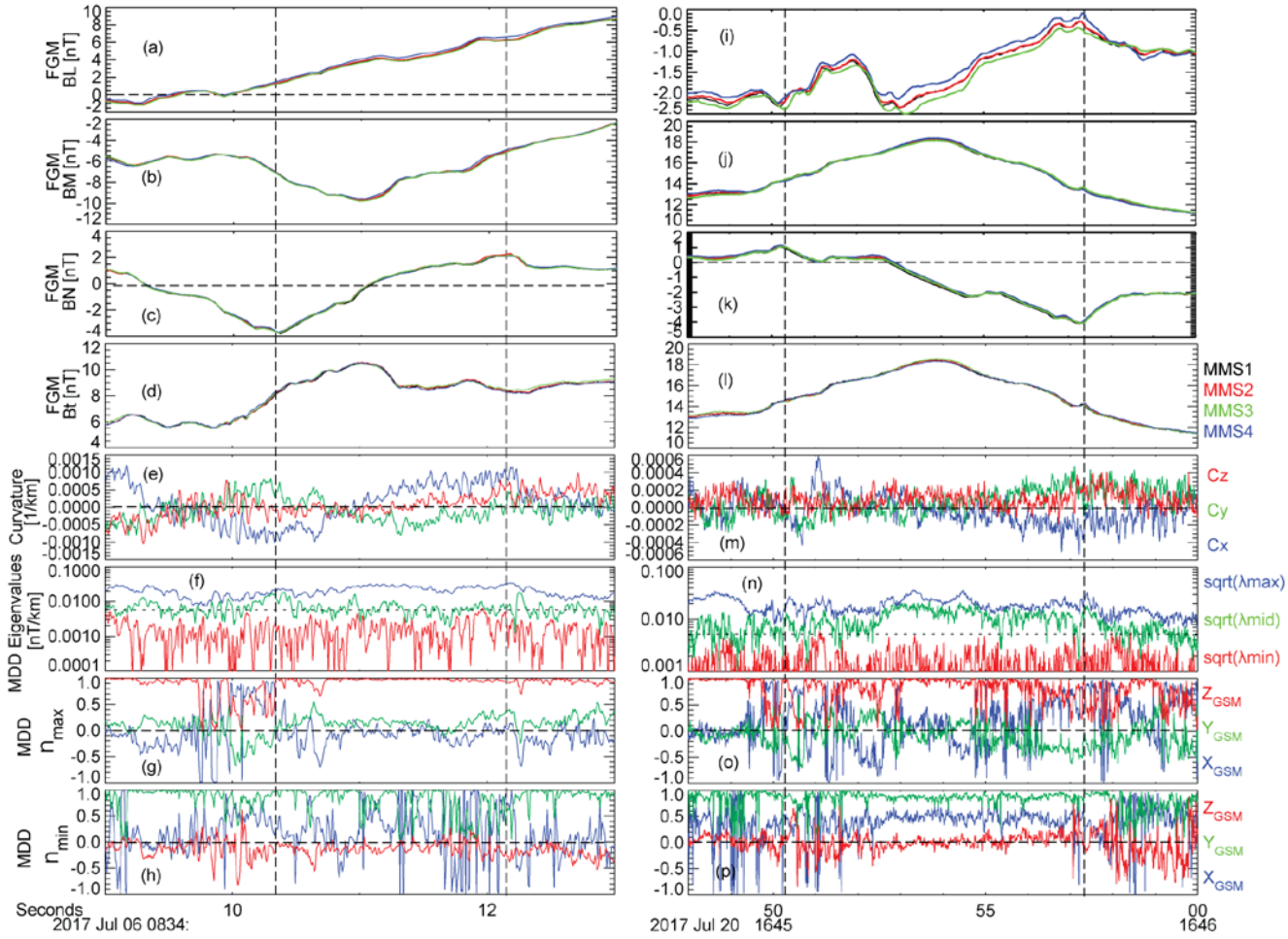

Figure 2. MMS multi-spacecraft observations of the ion-scale flux ropes. Left column: the July 6 event. Right column: the July 20 event. (a) and (i), B_X. (b) and (j), B_Y. (c) and (k), B_Z. (d) and (l), B_t. (e) and (m), local curvature of magnetic field line. (f) and (n), eigenvalues determined by the MDD, $\sqrt{\lambda_{max}}$ is in blue, $\sqrt{\lambda_{mid}}$ in green, $\sqrt{\lambda_{min}}$ in red. (g) and (o), the maximum eigenvector ($\hat{n}_{max}$). (h) and (p), the minimum eigenvector ($\hat{n}_{min}$). Magnetic field are in local coordinate. Curvature and eigenvectors are under GSM coordinate.

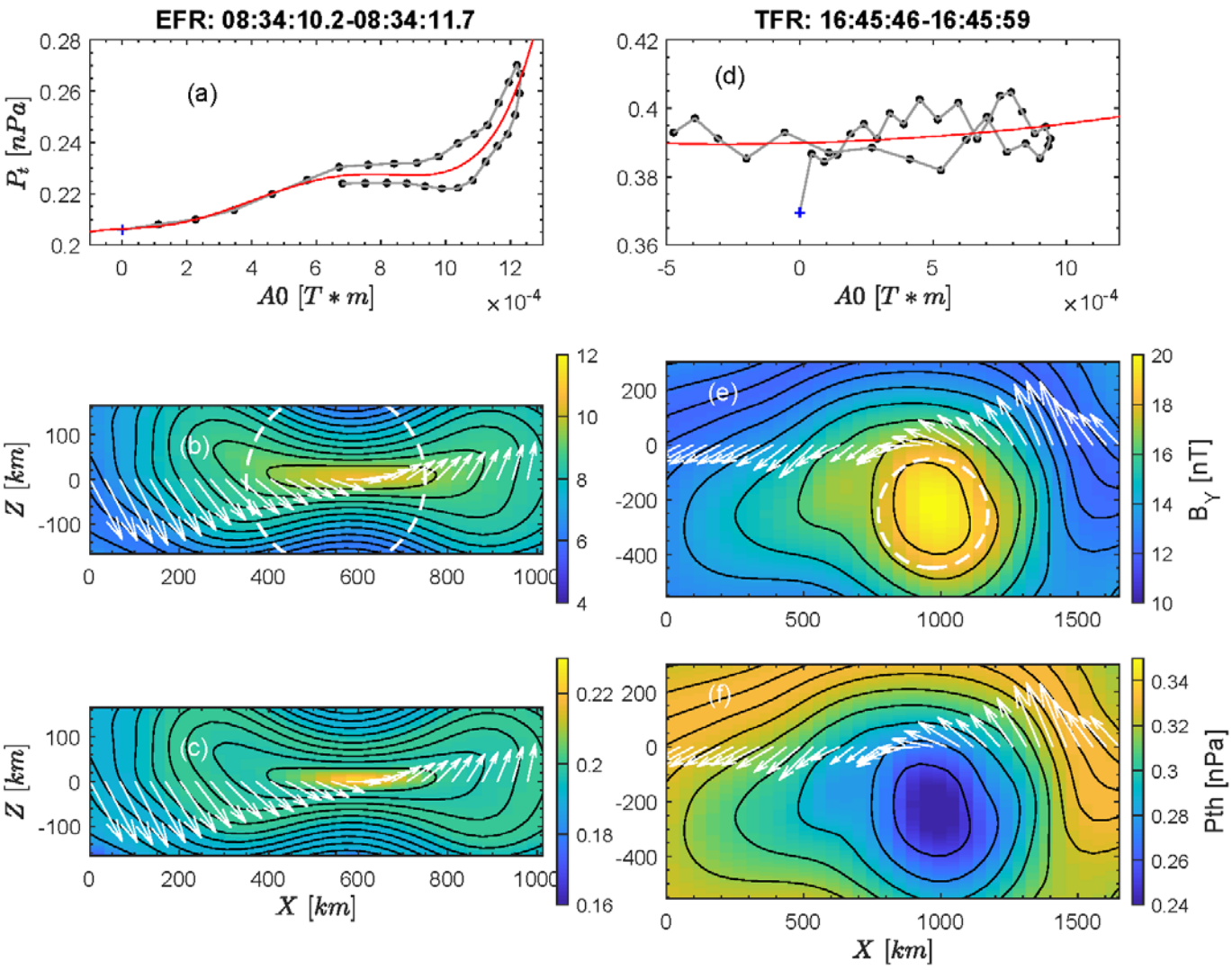

Figure 3. GS reconstruction of the ion-scale flux ropes. Left column: the July 6 event. Right column: the July 20 event. (a) and (d), transverse pressure P_t versus magnetic potential vector A_0. Black dots are the measurements from MMS1, red lines are polynomial fit of the dots. (b) and (e), color indicates axial field intensity (B_A) distributions in the plane perpendicular to the axes. Black lines are magnetic field lines. White arrows are the measured magnetic field components. White circles with radius of 200 km are plotted around the center. (c) and (f) are similar to (b) and (e) except that color indicates plasma thermal pressure (P_{th}). X and Z are the local coordinate.

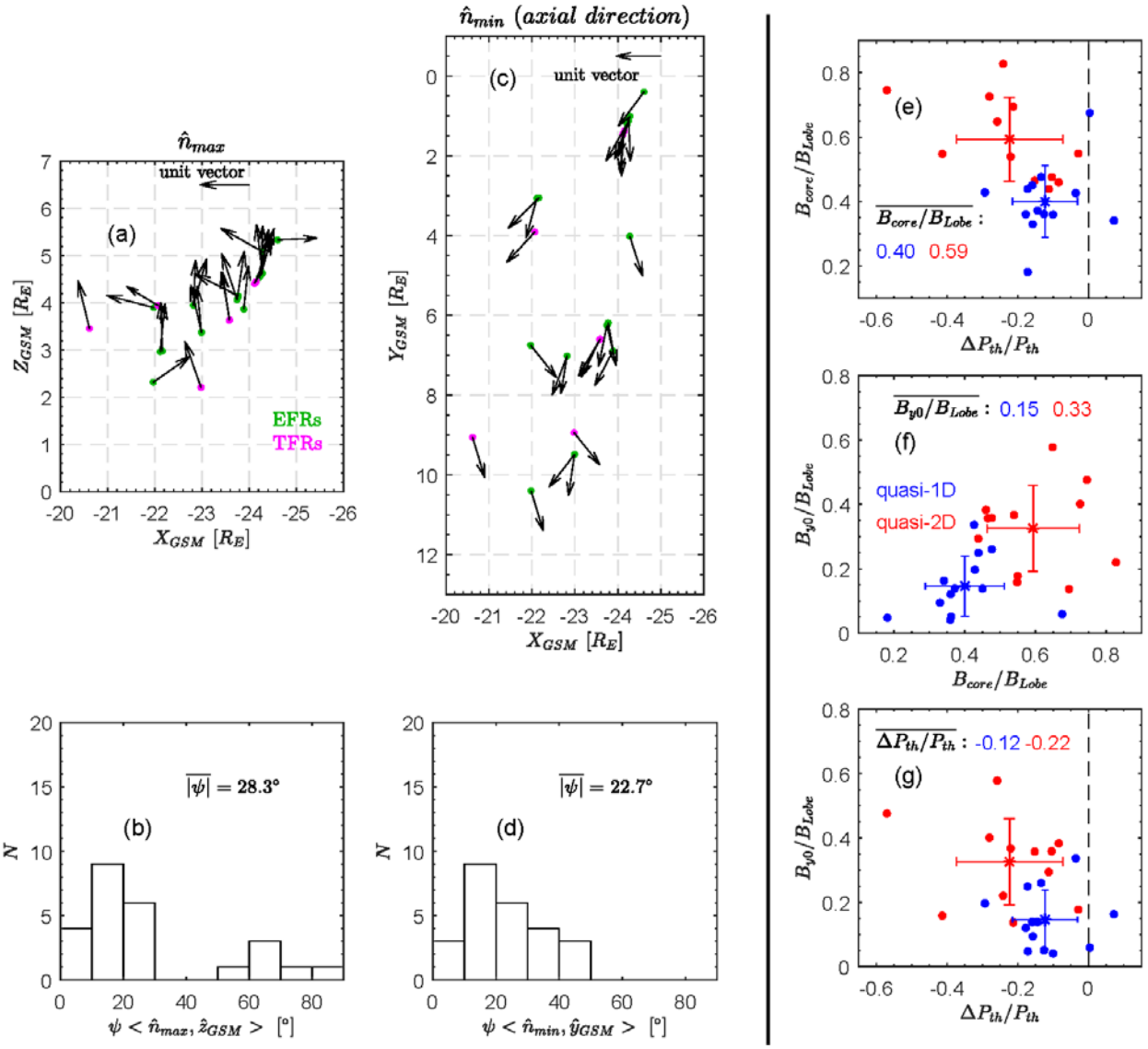

Figure 4. The statistical results of the ion-scale flux ropes. (a) and (c), the projection of $\hat{n}_{max}$ onto the $\hat{x}_{GSM}$-$\hat{z}_{GSM}$ plane and $\hat{n}_{min}$ onto the $\hat{x}_{GSM}$-$\hat{y}_{GSM}$ plane. (b) and (d), the separation angles between $\hat{n}_{max}$ and $\hat{z}_{GSM}$, and $\hat{n}_{min}$ and $\hat{y}_{GSM}$, respectively. (e) distribution of $B_{\rm core}/B_{\rm Lobe}$ and $\Delta P_{\rm th}/P_{\rm th}$. (f) distribution of $B_{\rm core}/B_{\rm Lobe}$ and $B_{\rm y0}/B_{\rm Lobe}$. (g) distribution of $\Delta P_{\rm th}/P_{\rm th}$ and $B_{\rm y0}/B_{\rm Lobe}$. $B_{\rm core}$ is core field of flux ropes, $B_{\rm Lobe}$ is lobe field, $P_{\rm th}$ is thermal pressure, $B_{\rm y0}$ is background guide field. Quantities of quasi-1D flux ropes are marked as blue dots, and quasi-2D flux ropes red dots. Both blue and red stars with errorbars are the means and standard deviations of each subsets.

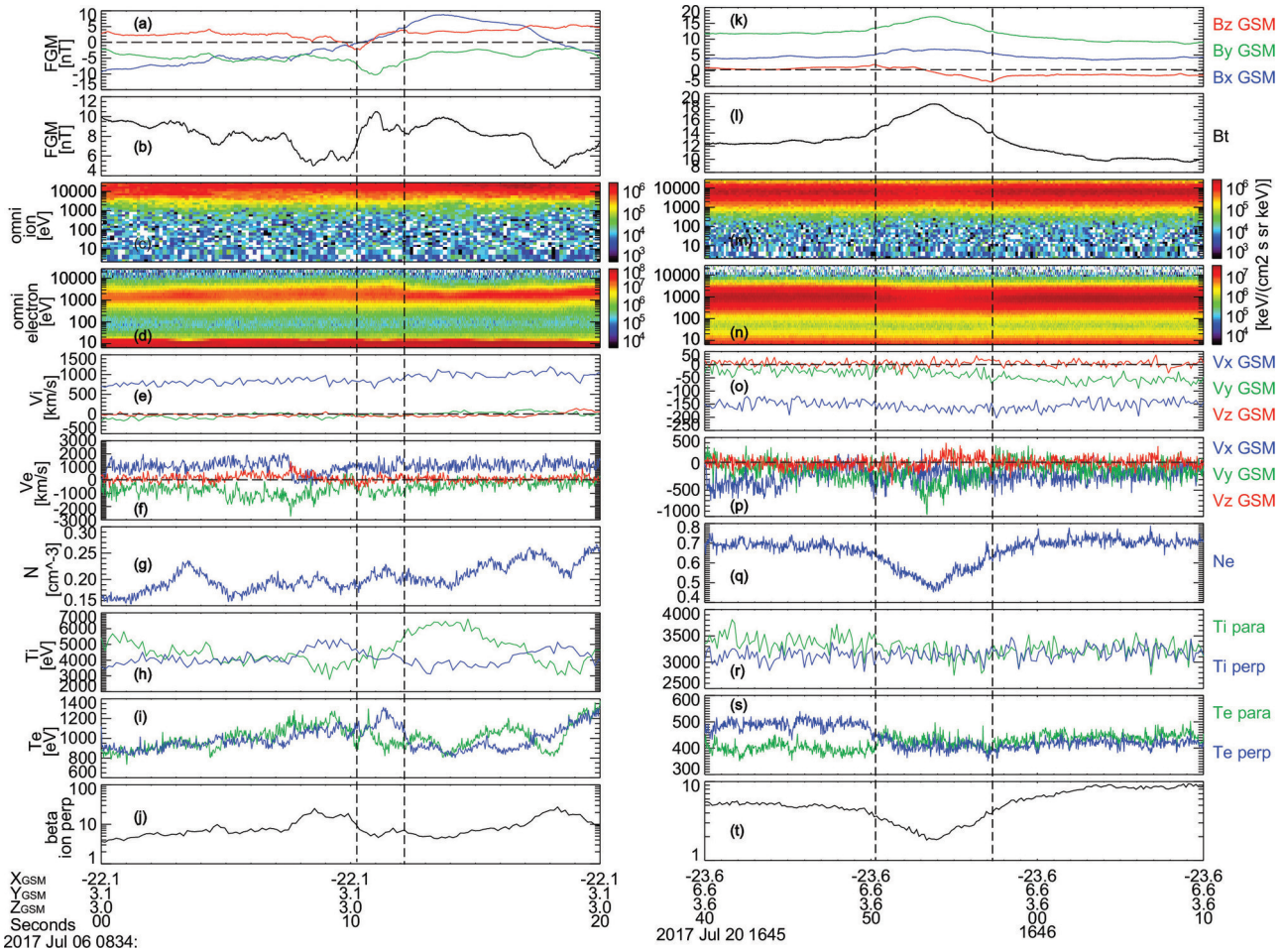

2019gl083301-f01-z-.eps

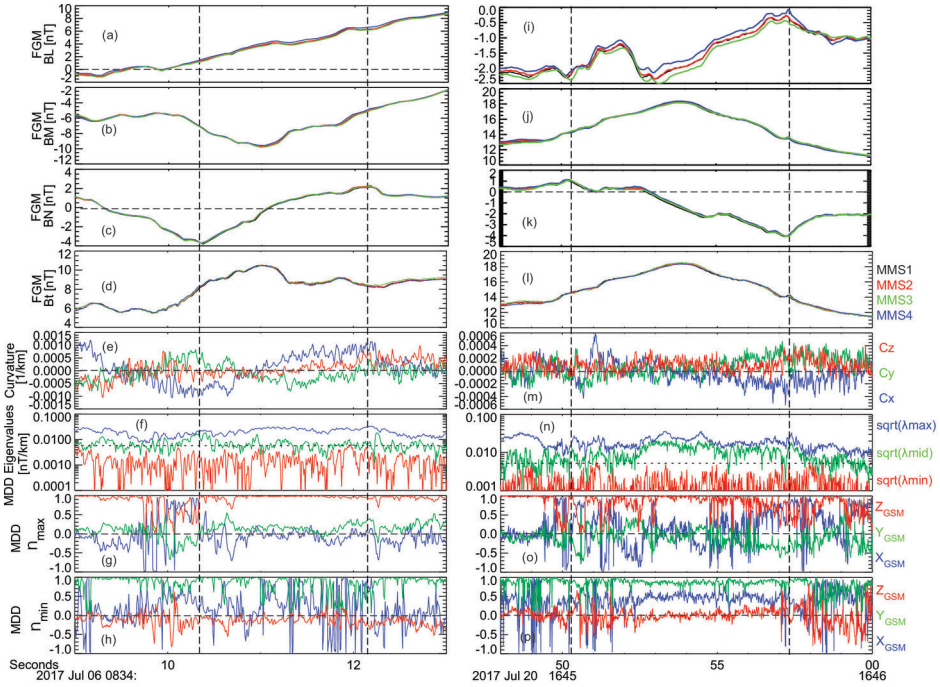

2019gl083301-f02-z-.eps

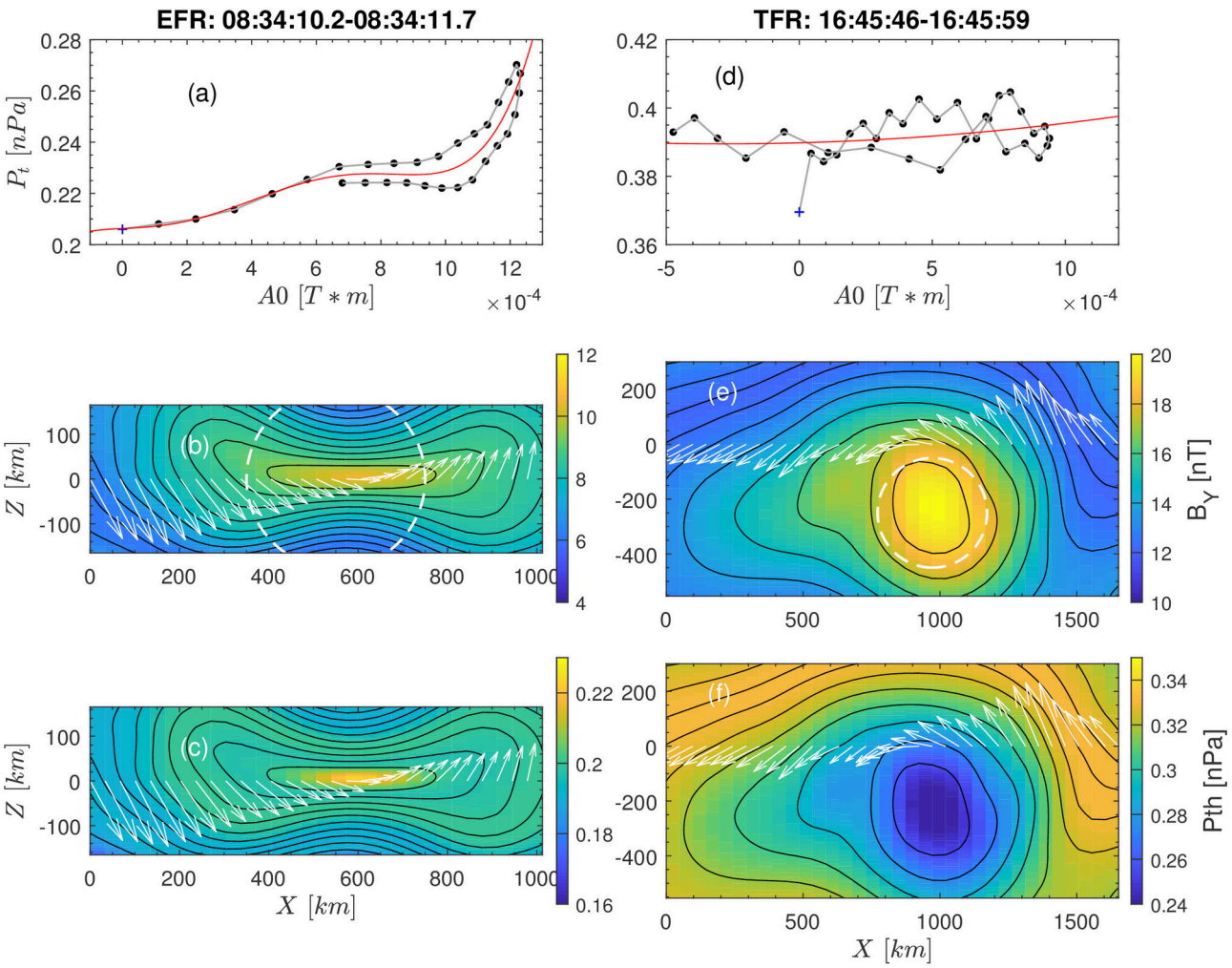

2019gl083301-f03-z-.eps

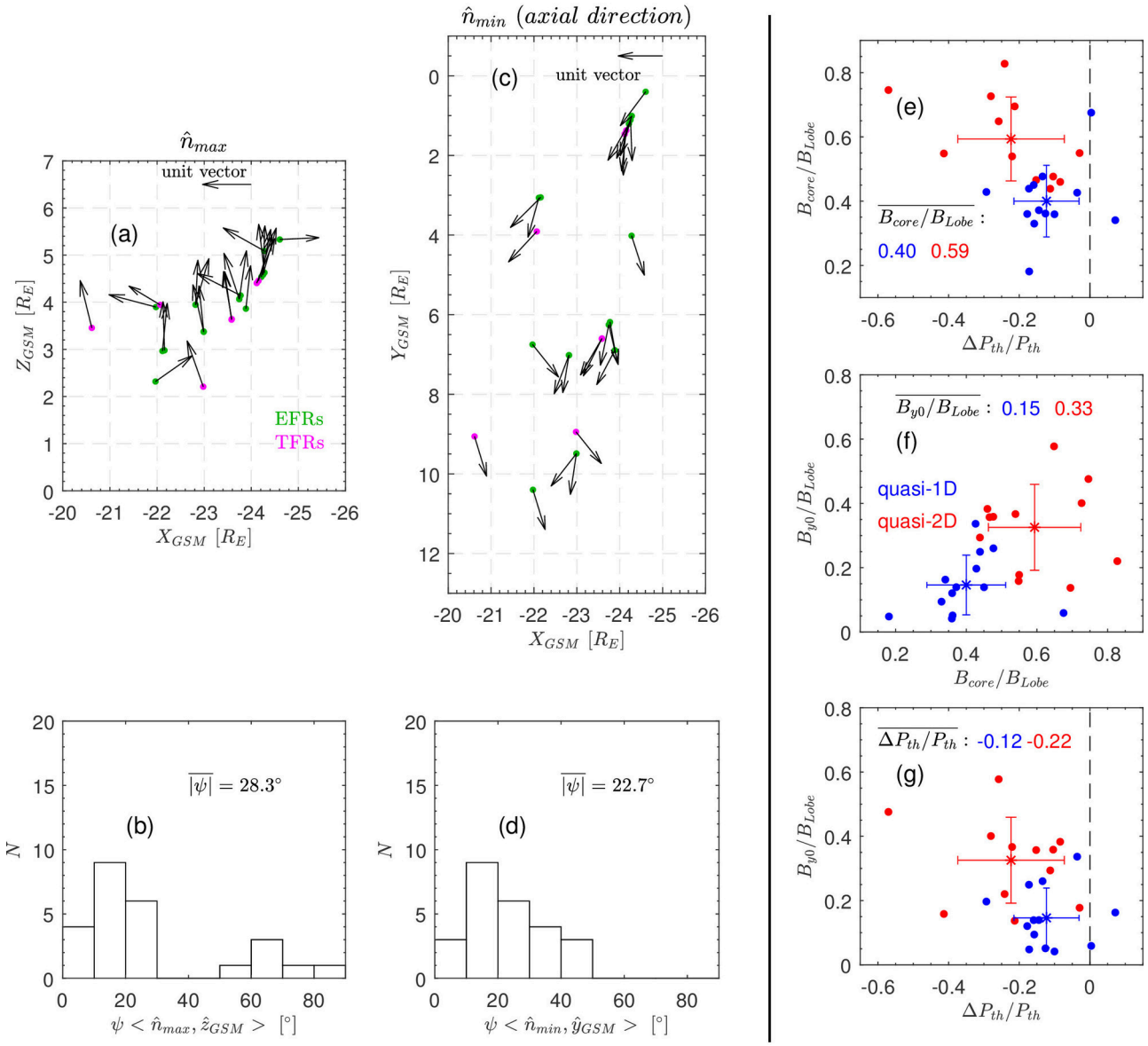

2019gl083301-f04-z-.eps